Available online at www.sciencedirect.com
SCIENCE DIRECT®
Journal of Magnetic Resonance 166 (2004) 69–75
JMR Journal of Magnetic Resonance
www.elsevier.com/locate/jmr

Pulsed optically detected NMR of single GaAs/AlGaAs quantum wells

Marcus Eickhoff* and Dieter Suter

Universität Dortmund, Fachbereich Physik, 44221 Dortmund, Germany

Received 24 June 2003; revised 11 September 2003

Abstract

While nuclear magnetic resonance (NMR) is one of the most important experimental tools for the analysis of bulk materials, the low sensitivity of conventional NMR makes it unsuitable for the investigation of small structures. We introduce an experimental scheme that makes NMR spectra of single, nanometer-sized quantum wells possible with excellent sensitivity and selectivity while avoiding the spectral broadening associated with some alternative techniques. The scheme combines optical pumping and pulsed radiofrequency excitation of the nuclei with time-resolved detection of the free induction decay through the polarization of the photoluminescence.

PACS: 76.60.-k; 78.55.Cr; 78.67.De

Keywords: ODNMR; Pulsed excitation; Quantum well; GaAs

1. Introduction

Nuclear magnetic resonance (NMR) is widely used for structural and dynamical studies of the properties of bulk materials [1,2], but the relatively low sensitivity of the technique makes it difficult to obtain information from small individual structures, such as semiconductor quantum wells. An important improvement to this situation is optical pumping [3], which transfers angular momentum from optical photons to the spins and can increase the spin polarization by several orders of magnitude [4]. This technique has been applied to bulk semiconductor samples [5] and has even made the detection of NMR spectra from single quantum wells possible [6].

An additional increase in sensitivity can be obtained by detecting the nuclear spins optically, via their effect on the polarization of the photoluminescence [5,7]. The NMR spectrum is then recorded by saturating one nuclear spin species with a cw radiofrequency (rf) field, either by sweeping the frequency or the strength of the external magnetic field. This approach has made possible, e.g., measurements of the Knight-shift [8] and quadrupole splittings [9,10]. Such optically detected NMR (ODNMR) experiments provide sufficient sensitivity to measure spectra of individual quantum wells [11–13].

In conventional NMR, cw measurements have largely been replaced by pulsed excitation and Fourier transformation of the free induction decay (FID) [1,2,14]. This approach increases the sensitivity and avoids artifacts like power broadening, since the spins evolve freely under their internal Hamiltonian during detection. Furthermore, the scheme can be generalized to multiple spectral dimensions [1].

Time-resolved optical detection of NMR in quantum wells was first used by Marohn et al. [15]. Their approach was to create a beat signal between two nuclear spin species. One species was spin locked by an rf field while the other was allowed to precess freely. The disadvantages of this approach include rather low sensitivity, poor spectral resolution, and the necessity to use a second spin species. Here we demonstrate that pulsed NMR experiments can be applied to individual

* Corresponding author. Fax: +49-2317553516.
E-mail addresses: marcus.eickhoff@uni-dortmund.de (M. Eickhoff), dieter.suter@physik.uni.dortmund.de (D. Suter).

1090-7807/$ - see front matter © 2003 Elsevier Inc. All rights reserved.
doi:10.1016/j.jmr.2003.09.009

nanometer-sized semiconductor heterostructures with excellent sensitivity, with a resolution only limited by the natural linewidth, and with potential extensions to multiple spectral dimensions.

2. Principle of experiment

We consider semiconductor quantum wells with a direct band gap that depends on its thickness. In addition, the degeneracy between light and heavy holes is lifted. The photoluminescence spectrum is dominated by the recombination of electrons with heavy holes at $k = 0$, and the absorption is also strongly enhanced at these wavelengths.

If circularly polarized light is incident on such a system, the polarization of the electron spins in the conduction band reaches a maximum when the excitation wavelength is within a few meV from the PL peak wavelength and drops off quickly outside the resonance. Hyperfine interaction (mostly Fermi contact) induces electron-nuclear spin flips that transfer some of the spin polarization to the nuclear spin system. Specifically, we consider GaAs, which contains ^{69}Ga, ^{71}Ga, and ^{75}As nuclear spins (all $I = 3/2$). Compared to thermal polarization, the optical pumping process increases the spin polarization by several orders of magnitude; under our experimental conditions ($T = 4\,\mathrm{K}$, $B_{\mathrm{ext}} = 1.4\,\mathrm{T}$), the nuclear spin polarization reaches 10–20% after 200 s.

During recombination, the remaining electron spin polarization is transferred to circular polarization of the luminescence photons. A measurement of the photoluminescence polarization is therefore a direct measure of the electron spin polarization.

In a magnetic field, the electron spins undergo Larmor precession. Averaged over the lifetime of the photoexcited electrons, one obtains a decrease in PL polarization, as described by the Hanle curve

$$\langle S_x \rangle = S_0 \frac{\Delta B^2 + B_{\mathrm{eff}}^2 \cos^2(\theta)}{\Delta B^2 + B_{\mathrm{eff}}^2}. \tag{1}$$

Here ΔB is the width of the Hanle curve, which depends on the electron g factor and the relaxation time, and S_0 the initial electron spin polarization. $B_{\mathrm{eff}} = B_{\mathrm{ext}} + B_{\mathrm{N}}$ is the effective magnetic field acting on the electrons, which is the sum of the external field and a nuclear field [16,17]. As shown in Fig. 1, θ represents the angle between this effective magnetic field and the direction of the initial electron spin polarization $\vec{S}_0$, which is the direction of the incident laser beam. The x-axis is defined by the direction of the measurement of the PL polarization. The nuclear field B_{N} describes the averaged hyperfine interaction (HFI) of the nuclei on the electron spin [17]. Its direction is parallel to the nuclear spin magnetization and its magnitude is proportional to the average hyperfine interaction and the polarization of the nuclear spins.

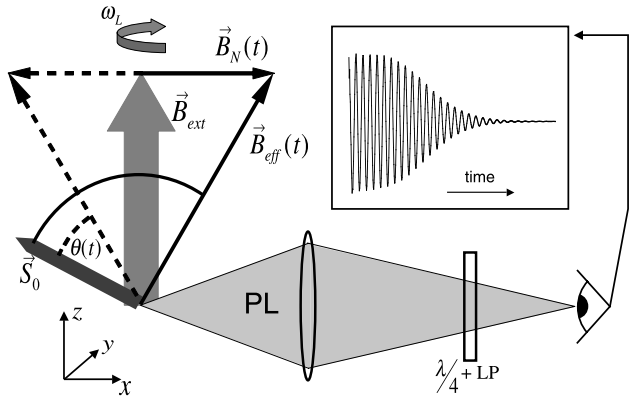

Fig. 1. Principle of the time-resolved, optically detected NMR: an rf pulse excites transverse nuclear spin magnetization that undergoes Larmor precession. The processing field B_{eff} modulates the angle θ between the initial electron spin polarization $\vec{S}_0$ and thereby the polarization of the emitted PL.

To demonstrate the principle of the experiment, we first consider the effect of a hypothetical spin 1/2 on the electron spin polarization. After the nuclear spin polarization is enhanced by optical pumping, a rf pulse tilts the nuclear spins by an angle ζ from the z-axis, creating transverse magnetization. The nuclear Zeeman interaction then causes precession of these spins at the Larmor frequency ω_{L} in the external magnetic field B_{ext} and therefore a modulation of the nuclear field. At the same time, the transverse magnetization decays (e.g., due to spin–spin interaction); we assume a Gaussian time-dependence for this relaxation process. The effective magnetic field felt by the electrons is then

$$\begin{aligned}\vec{B}_{\mathrm{eff}} &= \vec{B}_{\mathrm{ext}} + \vec{B}_{\mathrm{N}} \\ &= \begin{pmatrix} B_{\mathrm{N}} \sin(\zeta) \sin(\omega_{\mathrm{L}} t) \exp(-t^2 \ln(2) \delta^2) \\ B_{\mathrm{N}} \sin(\zeta) \cos(\omega_{\mathrm{L}} t) \exp(-t^2 \ln(2) \delta^2) \\ B_{\mathrm{ext}} + B_{\mathrm{N}} \cos(\zeta) \end{pmatrix}. \end{aligned} \tag{2}$$

This precession is much slower than the recombination time of the carriers relevant for the optical detection. We may therefore consider the magnitude and direction of the magnetic field felt by the electrons as constant during their lifetime.

The time dependence of the magnetic field direction is

$$\cos(\theta(t)) = \frac{\vec{S}_0 \cdot \vec{B}_{\mathrm{eff}}(t)}{|\vec{S}_0||\vec{B}_{\mathrm{eff}}(t)|}, \tag{3}$$

with the initial electron spin polarization

$$\vec{S}_0 = S_0 \begin{pmatrix} \sin(\phi) \\ 0 \\ \cos(\phi) \end{pmatrix}. \tag{4}$$

Here ϕ is the angle enclosed by the initial electron spin and B_{ext}. Eqs. (1)–(4) show that $B_{\mathrm{eff},x}$ is the only time dependent part relevant in the signal generation.

Combining Eqs. (1)–(4), we find the time dependence of the signal

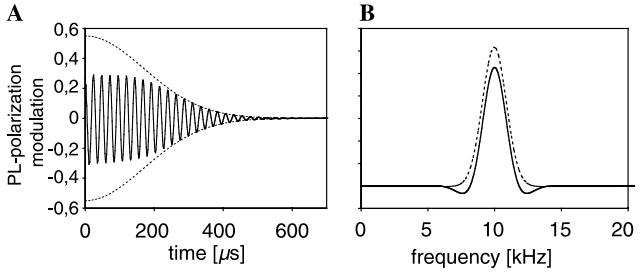

Fig. 2. (A) Simulated optical FID (solid line) and the envelope of a conventionally detected FID (dashed line), showing the damping of large signal amplitudes. (B) Real part of the frequency spectrum after Fourier transformation of the oFID (solid line) and of the normal FID (dashed line). The abscissa represents the frequency in the rotating frame of the rf.

$$\langle S(t)\rangle = S_0 \cdot \frac{\Delta B^2 + [B_{\mathrm{eff,x}}(t)\cdot\sin(\phi) + B_{\mathrm{eff,z}}\cdot\cos(\phi)]^2}{\Delta B^2 + |\vec{B}_{\mathrm{eff}}|^2}. \quad (5)$$

Fig. 2A depicts this time-dependence, which is comparable to the FID of conventional pulsed NMR. We therefore refer to this signal as an optically detected FID (oFID). As shown in Fig. 2A, its shape differs from the conventionally detected FID for short times. The difference originates from a nonlinearity in the optical sensitivity, which causes the signal to saturate when the nuclear field becomes comparable to the external magnetic field.

After bandwidth limitation to the Larmor frequency and Fourier transformation of the oFID the spectrum is obtained. The difference in the shape of conventional and optical FID are also visible in the spectrum (see Fig. 2B): the resulting lineshape is narrower than the conventional Gaussian shape, with small negative feet. This lineshape is similar to the lineshape generated by radiation damping, where higher currents in the NMR coil are damped, resulting in a nonlinearity between magnetization and induced signal [18].

According to Eq. (5), the sensitivity of the optically detected signal is proportional to the sine of the angle between the external magnetic field and the pump. At the same time, the nuclear magnetization established by optical pumping vanishes if the direction of the pump laser beam is perpendicular to the magnetic field (Voigt configuration) and reaches its maximum when the two directions coincide (Faraday configuration). The overall sensitivity therefore reaches a maximum at 45° and vanishes at 0° and 90°.

3. Experimental details

As a test sample, we used a multiple quantum well structure grown by molecular beam epitaxy (MBE). The thickness of the quantum wells varied from 2.8 to 38 nm and they were separated by 39 nm wide $Al_{0.3}Ga_{0.7}As$ barriers. Fig. 3 shows the photoluminescence (PL) spectrum of the sample, which contains well separated resonance lines for the individual quantum wells.

The sample was mounted on the cold finger of a helium flow cryostat and cooled to liquid helium temperatures between the poles of an iron magnet, capable of generating magnetic fields up to 1.4 T. The magnetic field was oriented at an angle of $\phi = 70°$ from the growth direction of the sample. The sample was illuminated by circularly polarized laser light resonant with the absorption line of excitons in one of the quantum wells. The laser light with a power of 40 mW propagated parallel to the growth direction ([0 0 1]-direction) of the sample and was focused to a diameter of 50 μm.

The emitted PL was collected by a collimation lens of 50 mm diameter and 100 mm focal length and analyzed by a quarter wave plate and a linear polarizer. Thus, only the light with one defined circular polarization was focused on the active area of an avalanche photo diode (APD). The APD has a bandwidth of 10 MHz and a sensitivity of 1.6×10^6 V/W including an internal gain of 30. The signal of the APD was electronically filtered with a passband of 8–12 MHz. Shot noise of the scattered laser light and instabilities of the light intensity limit the signal-to-noise ratio (SNR). These contributions sum to a noise level of 2 nW, which is six-times bigger than the 0.35 nW noise equivalent power of the APD circuit.

The radiofrequency was applied to the sample by a set of two coils in Helmholtz-configuration. With a capacitor these coils were tuned to a resonance frequency of ~10 MHz. The circuit was driven by a 100 W power amplifier. The resonance condition for one of the nu-

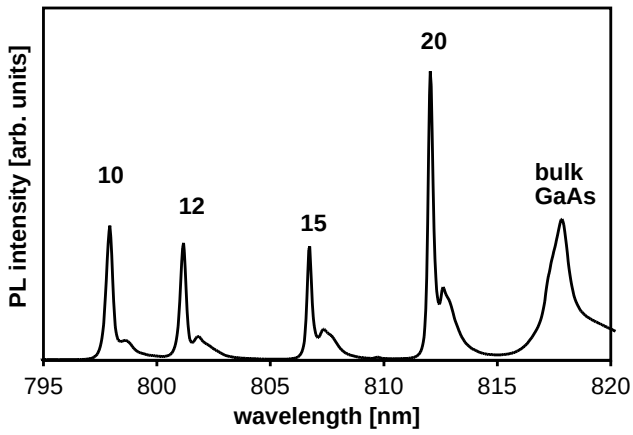

Fig. 3. PL spectrum of the quantum well sample containing quantum wells of different widths. Each emission line is labeled with the width in nanometer of the appendant quantum well. The sample was optically excited with 785 nm light.

clear isotopes was established by adjusting the magnetic field strength. In contrast to conventional NMR, where the signal is detected through the induction in the RF-coil, the optical detection can start instantaneously during the applied pulse, without any delay caused by saturation of the pre-amplifier. The light irradiating the sample was used for optical pumping and for detecting the NMR signal after the pulse, and thus applied resonantly with the absorption line of one quantum well and continuously during the whole experiment. Scattered light contributes some 50% to the total signal. Since it is a constant (DC) signal, it does not contribute to the NMR signal, which is obtained through phase-sensitive detection at the Larmor frequency.

4. Signal

As an example for a resulting spectrum, Fig. 4 shows the ^{75}As spectrum of a 15 nm wide quantum well. It was measured by optically pumping the sample for 160 s and applying a 6 μs rf pulse to the sample. The dots indicate the experimental data, while the solid line was calculated with Eqs. (2) and (5) and the parameters given in the figure caption.

The spectrum shows the typical three line spectrum of a spin $I = 3/2$. While bulk GaAs does not show quadrupole splittings, they are common in heterostructures, where mechanical strain and electric fields lift the equality of the three Δm_I nuclear spin-flip transition energies [10]. Apart from the splitting, the satellites show inhomogeneous broadening; the width of the satellite lines is 4 kHz, compared to 2 kHz for the central transition, which is not affected by the quadrupole coupling in first order.

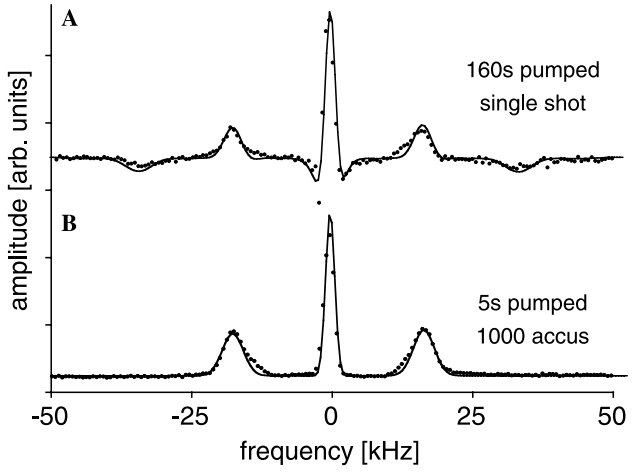

Fig. 4. Pulsed spectra of arsenic. Dots represent experimental data and the solid lines the calculated spectra. The polarization was established by optically pumping for (A) 160 s and (B) 5 s. The quadrupole splitting is 17 kHz. The FWHH for the central and the satellite lines are 2 and 4 kHz, respectively. The external magnetic field was set to 1.38 T and the rf frequency was 9.96 MHz.

Fig. 4 clearly shows the lineshape distortions that we discussed in the theoretical section: the central transition has negative wings, and additional satellites show up at twice the quadrupole splitting. These effects can be avoided by either choosing a short pumping time or a small flip angle pulse, to remain in the linear regime of the detection system. This is demonstrated in Fig. 4B, where a smaller magnetization was prepared by reducing the pumping time to 5 s.

The spectrum of Fig. 4A originates from some 10^{11} nuclear spins. The measured SNR is 80 for the highest peak in the spectrum. To achieve a comparable SNR in single shot, low temperature experiments with an ordinary NMR spectrometer, a minimum of 10^{16} ^{75}As nuclei are required, significantly more than the quantum well contains.

To describe a spin 3/2 system like all three isotopes present in GaAs we expand the time dependence of the effective field in Eq. (2) to three single transitions with different amplitudes, linewidths, and frequencies. After deconvolution with the responsivity of the detection setup, we found that the observed lineshapes could well be modeled by Gaussian functions. The satellites are split from the central line by quadrupole interaction due to mechanical strain and electric fields [10]. In the spectra of Fig. 4, this splitting between the central and satellite lines is 17 kHz. The full width at half height of the central and satellite lines are 2 and 4 kHz, respectively. The broadening of the satellites indicates a distribution of strain and/or electric fields in the quantum well.

The experiment can be performed with any nuclear spin that can be resonantly excited. This is shown in Fig. 5, where the other relevant isotopes are measured separately. The NMR signals of ^{69}Ga and ^{71}Ga were measured at the same sample position; they show quadrupole splittings of 5.2 and 3.4 kHz, respectively. The ratio of the splittings for the two gallium isotopes scales with their quadrupole moments.

The establishment of nuclear polarization during the optical pumping process can be described by a relaxation time T_{1e} of 55 s. With a higher nuclear polarization and correspondingly bigger nuclear fields precessing during resonance, the distortion of the resonance shape due to the optical detection increases. Fig. 4 shows two spectra for different pumping duration and thus, different nuclear fields. For a time much shorter than T_{1e} the shape of the resonance signal looks like a conventional NMR signal. For higher spin polarizations, the lineshape changes, as discussed in Section 2.

The pulsed excitation used here allows one to determine the spin temperature of the optically pumped nuclei. If the spin polarization exceeds a few percent, the population differences for the three dipole-allowed transitions become unequal. For positive spin temperature, the population difference is largest for the transition

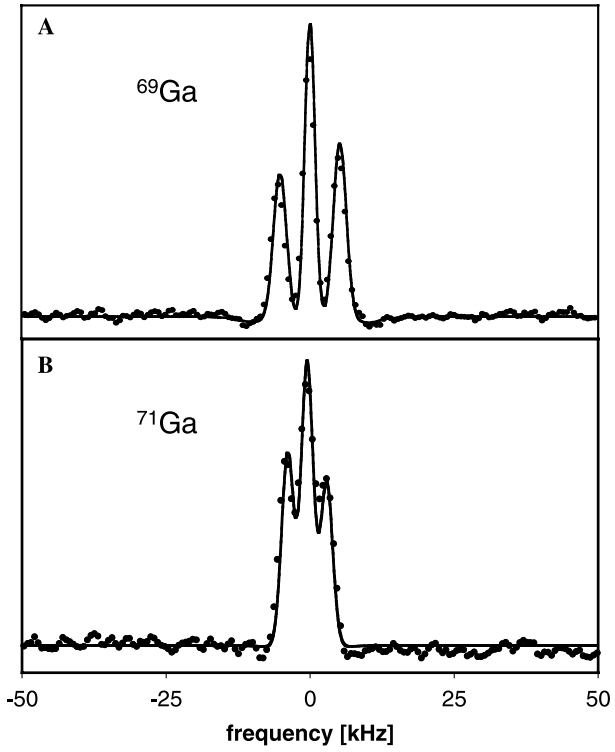

Fig. 5. Optically detected pulsed NMR spectra of (A) ^{69}Ga and (B) ^{71}Ga from the 15 nm wide quantum well. The quadrupole splittings are 5.2 and 3.4 kHz, respectively. Each spectrum was obtained by Fourier transformation of the average of 9 oFID's. Before each scan, the spins were optically pumped for 600 s.

between the two lowest states. If a small flip angle is used for excitation, the resulting spectrum is asymmetric.

Fig. 6 shows the flip angle dependence of the two outer lines of the ^{75}As spectrum. For flip angles $<90°$, the high frequency line is stronger, while the low frequency line becomes larger when the flip angle exceeds $\pi/2$. The experimental data points agree quite well with the theoretical curves, which were calculated for a spin temperature of 2 mK.

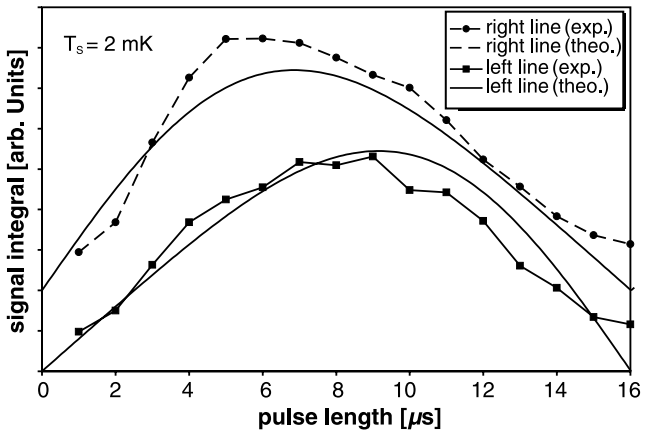

Fig. 6. Dependence of the left and right satellite signal integrals on the pulse duration. The asymmetry of the flip angle dependence is caused by a spin temperature of 2 mK. The right satellite signal integrals are vertically shifted in this figure.

5. Multiple quantum wells

Layered heterostructure samples contain multiple thin films with the same nuclear isotopes as the substrate. In conventional NMR, the signal from the substrate always dominates that of the quantum wells unless specific relaxation properties of nuclei in the quantum wells are exploited [19–21]. Optical pumping combined with conventional detection [6,22–24] can increase the signal contributions from quantum films to levels comparable to that of the substrate.

The optical detection, which further increases the sensitivity, provides an additional path to background suppression, which is well compatible with the optical pumping. We demonstrate this feature for our experiment by comparing the spectra from different quantum wells in a multiple quantum well sample. Fig. 7 shows on the left-hand side a part of the PL spectrum of this sample. The five peaks originate from five quantum wells of different thickness, which are separated by 30 nm barriers.

Since the optical pumping efficiency depends strongly on the laser wavelength, tuning the laser to one of the resonances allows one to select the quantum well to be investigated. The right-hand side of the figure contains the resulting NMR spectra of the five quantum wells. The spectra show significant differences in the positions, widths, and amplitudes of the three resonance lines, indicating that each of them is associated with a different quantum well. The signal size decreases with the width

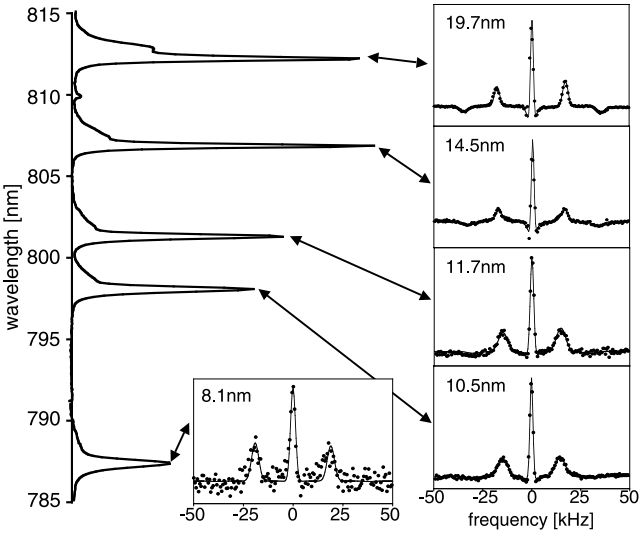

Fig. 7. The PL spectrum of the sample containing single quantum wells of different widths is shown on the left side. The pulsed ODNMR spectra were recorded with the pump laser exciting the sample resonant with the quantum well of the width noted in each spectra.

of the quantum wells as the reduced absorption cross-section of the thinner quantum wells reduces the number of photoelectrons available for optical pumping and detection. Furthermore, the effective g-factor for the electrons also depends on the thickness of the quantum well. For quantum wells close to 8 nm, it shows a zero crossing [25]. Small g-factors correspond to large widths of the Hanle curve and therefore to small signal.

Barrett et al. [6] have shown for directly detected OPNMR that the NMR signal of the quantum wells is strongly correlated to their absorption and that no detectable nuclear polarization occurs if the pump light is not resonant with the quantum well. Here in addition the quantum wells are selected by the enhanced emission of PL, if they are resonantly excited. The emitted PL of the resonant quantum well exceeds the PL of the other quantum wells and of the bulk GaAs substrate.

To verify that the signal originates only from the excited quantum well, we measured the NMR signal as a function of the laser wavelength as it was tuned over the resonance of a quantum well. As shown in Fig. 8, the signal amplitude shows a clear resonant behavior and quickly drops off as the laser is detuned from the center of the resonance line. This indicates that the NMR signal can only be measured for resonant excitation and that the observed signal always originates only from the resonantly irradiated quantum well. Similarly, contributions from the nuclei in the GaAs substrate can be excluded.

In addition to the selection mechanisms discussed here, it is possible to filter the PL by passing it through a spectrometer. This has the additional advantage that it can be used for eliminating scattered laser light, which contributes to the noise. The disadvantage of the optical spectrometer is that it reduces the detected PL intensity. Under typical experimental conditions, the spectrometer can well be omitted.

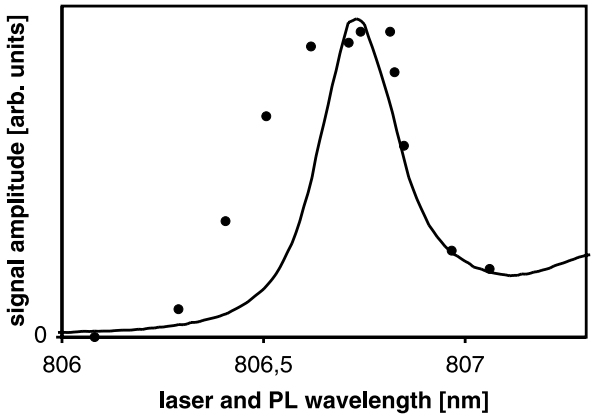

Fig. 8. Amplitude of the NMR signal as a function of the laser wavelength. Dots represent the observed NMR signal amplitudes and the solid line is the PL intensity, superimposed to show the selectivity of the NMR detection. This PL measurement was performed by scanning the detection wavelength while the excitation was fixed at 690 nm.

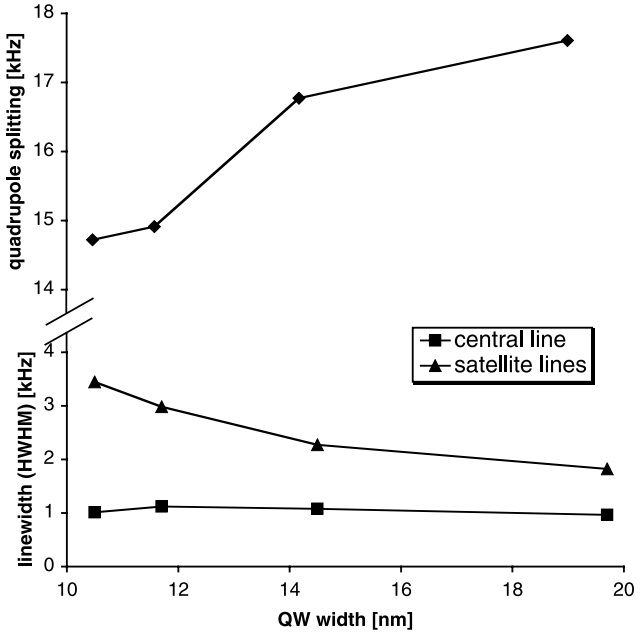

Fig. 9. In the upper part the quadrupole splitting for each quantum well is shown. The different splittings are due to a dependence of the EFG on the position in the sample. The lower part shows the line width dependence of the central and satellite resonance lines on the width of the quantum well. The linewidth of the satellite line has a clear dependence on the quantum well width.

The spectra of the different quantum wells presented in Fig. 7 show significant variations between the quantum wells, which are separated by 30 nm barriers. In Fig. 9, we summarize the variation of the two most interesting parameters, the quadrupole splitting and the width of the three resonance lines. While the splitting increases with the width of the quantum well, the width of the central line remains constant and the width of the satellites decreases. The broadening of the satellite lines is a measure of the distribution of quadrupole splittings, which does not affect the central transition. The increase of the linewidth for the thinner quantum wells shows that the variation of EFG values is larger in the thinner quantum wells. This may indicate that disorder is larger near the quantum well–barrier interface, which becomes more important in thinner wells.

The magnitude of the quadrupole splitting of each quantum well depends on its distance to the surface of the sample. This is caused by a variation of the electrical fields and/or mechanical stress in growth direction [10].

6. Summary and conclusions

The experimental scheme introduced here allows one to measure time-resolved NMR spectra of individual semiconductor quantum wells. In many cases, spectra with good signal-to-noise ratio could be obtained from single oFID's, dramatically reducing the measurement

time compared to other techniques. At the same time, the linewidth of these spectra is only limited by the natural linewidth of the sample, as the spins undergo free precession during detection. The experiment was applied to all three nuclear isotopes of GaAs and extensions to other materials with direct band-gap should be straightforward.

Like in conventional NMR, pulsed experiments offer, in addition to the reduced measurement time, increased flexibility in the design of experiments. Examples for pulsed experiments that offer higher information content include spin-echo or double-resonance experiments. Since single scans are measured during less than 1 ms, spin diffusion is strongly suppressed and the measured spectra originate only from nuclei within the localized excitons.

Two-dimensional experiments are also possible and could be used, e.g., to extend the measurement range to larger areas by introducing delays for spin diffusion to connect the nuclear spins within the excitons to neighboring areas. This should allow us to measure correlation lengths of structural and electronic inhomogeneities in the quantum wells with excellent resolution.

Acknowledgment

We acknowledge the loan of the sample by Prof. Wieck, Ruhr University of Bochum.

References

[1] R.R. Ernst, G. Bodenhausen, A. Wokaun, Principles of Nuclear Magnetic Resonance in One and Two Dimensions, Oxford University Press, Oxford, 1997.
[2] A. Abragam, Principles of Nuclear Magnetism, Oxford Science Publications, Oxford, 1994.
[3] F. Meier, B.P. Zakharchenya (Eds.), Optical Orientation, North-Holland, Amsterdam, 1984.
[4] G. Lampel, Phys. Rev. Lett. 20 (1968) 491.
[5] T. Pietraß, A. Bifone, J. Krüger, J.A. Reimer, Phys. Rev. B 55 (1997) 4050.
[6] S.E. Barrett, R. Tycko, L.N. Pfeiffer, K.W. West, Phys. Rev. Lett. 72 (1994) 1368.
[7] D. Paget, Phys. Rev. B 25 (1982) 4444.
[8] M. Krapf, G. Denninger, H. Pascher, Solid State Commun. 78 (1991) 459.
[9] D.J. Guerrier, R.T. Harley, Appl. Phys. Lett. 70 (1997) 1739.
[10] M. Eickhoff, B. Lenzmann, D. Suter, S.E. Hayes, A.D. Wieck, Phys. Rev. B 67 (2003) 085308.
[11] G.P. Flinn, R.T. Harley, M.J. Snelling, A.C. Tropper, T.M. Kerr, Semicond. Sci. Technol. 5 (1990) 533.
[12] M. Schreiner, H. Hochstetter, H. Pascher, S.A. Studenikin, J. Magn. Reson. 124 (1997) 80.
[13] S.W. Brown, T.A. Kennedy, E.R. Glaser, D.S. Katzer, J. Phys. D 30 (1997) 1411.
[14] R.R. Ernst, W.A. Anderson, Rev. Sci. Instrum. 37 (1966) 93.
[15] J.A. Marohn, P.J. Carson, J.Y. Hwang, M.A. Miller, D.N. Shykind, D.P. Weitekamp, Phys. Rev. Lett. 75 (1995) 1364.
[16] B.P. Zakharchenya, V.K. Kalevich, V.D. Kul'kov, V.G. Fleisher, Sov. Phys. Solid State 23 (1981) 810.
[17] D. Paget, G. Lampel, B. Sapoval, V.I. Safarov, Phys. Rev. B 15 (1977) 5780.
[18] X.-A. Maou, C.-H. Ye, Concepts Magn. Reson. 9 (1997) 173.
[19] S. Melinte, N. Freytag, M. Horvatic, C. Berthier, L.P. Levy, V. Bayot, M. Shayegan, Phys. Rev. Lett. 84 (2000) 354.
[20] S. Melinte, N. Freytag, M. Horvatic, C. Berthier, L.P. Levy, V. Bayot, M. Shayegan, Phys. Rev. B 64 (2001) 085327.
[21] M. Horvatic, C. Berthier, Int. J. Mod. Phys. B 16 (2002) 3265.
[22] S.E. Barrett, G. Dabbagh, L.N. Pfeiffer, K.W. West, R. Tycko, Phys. Rev. Lett. 74 (1995) 5112.
[23] P. Khandelwal, N.N. Kuzma, S.E. Barrett, L.N. Pfeiffer, K.W. West, Phys. Rev. Lett. 81 (1998) 673.
[24] A.E. Dementyev, P. Khandelwal, N.N. Kuzma, S.E. Barrett, L.N. Pfeiffer, K.W. West, Solid State Commun. 119 (2001) 217.
[25] M.J. Snelling, E. Blackwood, C.J. McDonagh, R.T. Harley, C.T.B. Foxon, Phys. Rev. B 45 (1992) 3922.